Site Response of the Ganges Basin inferred from re-evaluated Macroseismic Observations from the 1897 Shillong, 1905 Kangra and 1934 Nepal earthquakes.

Susan E. Hough and Roger Bilham

Abstract: We investigate details of the intensity distributions throughout the Punjab, Ganges and Brahmaputra river valleys following the Ms=8.1 Shillong (1897), Ms=7.8 Kangra (1905), and Ms=8.2 Nepal/Bihar (1934) earthquakes. For each earthquake we subtract the observed MSK intensities from a synthetic intensity derived from an inferred planar rupture model of the earthquake, combined with an attenuation function derived from instrumentally recorded earthquakes. The resulting residuals are contoured to identify regions of anomalous intensity caused primarily by local site effects. Observations indicative of liquefaction are treated separately from other indications of shaking severity lest they inflate inferred residual shaking estimates. Despite this precaution we find that intensites are 1-3 intensity units higher near the major rivers, as well as at the edges of the Ganges basin. We find evidence for a post-critical Moho reflection from the 1897 and 1905 earthquakes that raises intensities 1-2 units at distances of the order of 150 km from the rupture zone, and we find that the 1905 earthquake triggered a substantial subsequent earthquake at Dehra Dun, at a distance of approximately 150 km. Four or more M=8 earthquakes are apparently overdue in the region based on seismic moment summation in the past 500 years. Results from the current study permit anticipated intensities in these future earthquakes to be refined to incorporate site effects derived from dense macroseismic data.

Introduction: Several recent studies have provided new estimates of magnitude, rupture parameters, and/or shaking intensity for the 1897 Assam and 1905 Kangra earthquakes in northern India (e.g., Ambraseys and Bilham, 2000; Bilham and England, 2001, Ambraseys and Douglas, 2003). Rupture parameters of the 1934 Bihar-Nepal earthquake are less well-constrained, although a reasonably precise instrumental magnitude is available for this event (Chen & Molnar, 1977). The dense spatial coverage of macroseismic data from all three events (Figure 1) provides substantial additional information about the distribution of shaking in the alluvial plains of northern India that can be used to evaluate past and future great Himalayan earthquakes as well as to address unresolved general issues related to both events.

The magnitudes of the 1897 and 1905 earthquakes listed in early catalogues vary by 0.5 magnitude units. A recently re-evaluated instrumental seismic magnitude indicate the 1897 earthquake was Ms=8.0±0.1 (Ambraseys, 2000), with a seismic moment of Mw=8.1±0.1 calculated from geodetic data (Bilham & England, 2001). The 1905 earthquake was Ms=7.8±0.05 (Ambraseys and Bilham, 2000), Mw 7.8 (Ambraseys and Douglas 2004). For the 1934 earthquake Chen and Molnar (1977) calculate Mw=8.2, and Ambraseys and Douglas (2004) calculate Mw8.1.

The observed shaking intensities for the 1897 earthquake were originally evaluated by Oldham (1899), for the 1905 earthquake by Middlemiss (1905, 1910), and for the 1934 earthquake by Dunn et al., (1939). Their observations were supplemented by additional accounts found in newspapers, government reports and other materials, and have been re-evaluated using the MSK scale by Ambraseys

and Bilham (2003) and Ambraseys and Douglas (2004). In all 282 unequivocal MSK intensities were assigned for the 1897 earthquake, 523 for the 1905 earthquake, and 806 for the 1934 earthquake. The new evaluations take into account building styles and ignore accounts for which reliable intensities cannot be assessed. In particular, locations where damage was associated with liquefaction were not included in assessments of intensity. Liquefaction tends to occur on saturated sediments over a range of moderate to high intensities, resulting in building damage caused by foundation failure, rather than by direct shaking effects. It is typically impossible to assign a precise intensity to these observations. Notwithstanding this limitation, the available of carefully interpreted, dense macroseismic observations provide considerable constraint on the distribution of shaking generated by these three large earthquakes.

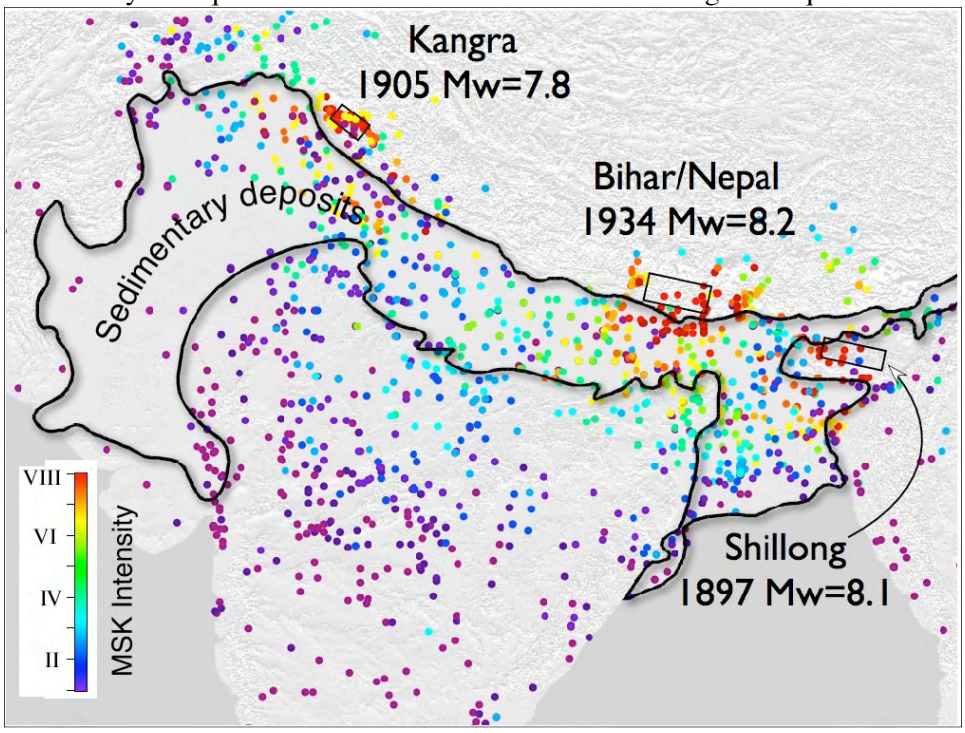

Figure 1 Locations of the three earthquakes discussed with their more than 1000 re-evaluated MSK intensities from all three events from Ambraseys and Douglas (2003). The region of river flood plains outlined in black embraces the core of the Indian Craton to its south. Recent fold belts surround this region to the west, north and east.

Rupture Geometries

The rupture geometries of each of the three earthquakes are associated with varying degrees of uncertainty, which we evaluate as follows:

12 June 1897 Shillong Mw8.1

Geodetic and geological data provide strong constraints on rupture geometry of the 1897 Shillong earthquake, indicating 16±5 m of reverse slip on a 110±10-km ESE fault, (Bilham and England, 2001) corresponding to a Mw=8.1±0.1 earthquake (Table1). The rupture appears to have slipped on a 50±5° SSW dipping fault from 35 km to 9 km depth, extending through much of the crust. This subsurface slip stressed the shallower regions of the Shillong plateau resulting in 10 m of normal faulting on the Chedrang fault (Oldham, 1899) and numerous aftershocks, some of which did further damage. It is assumed that rupture propagated up-dip

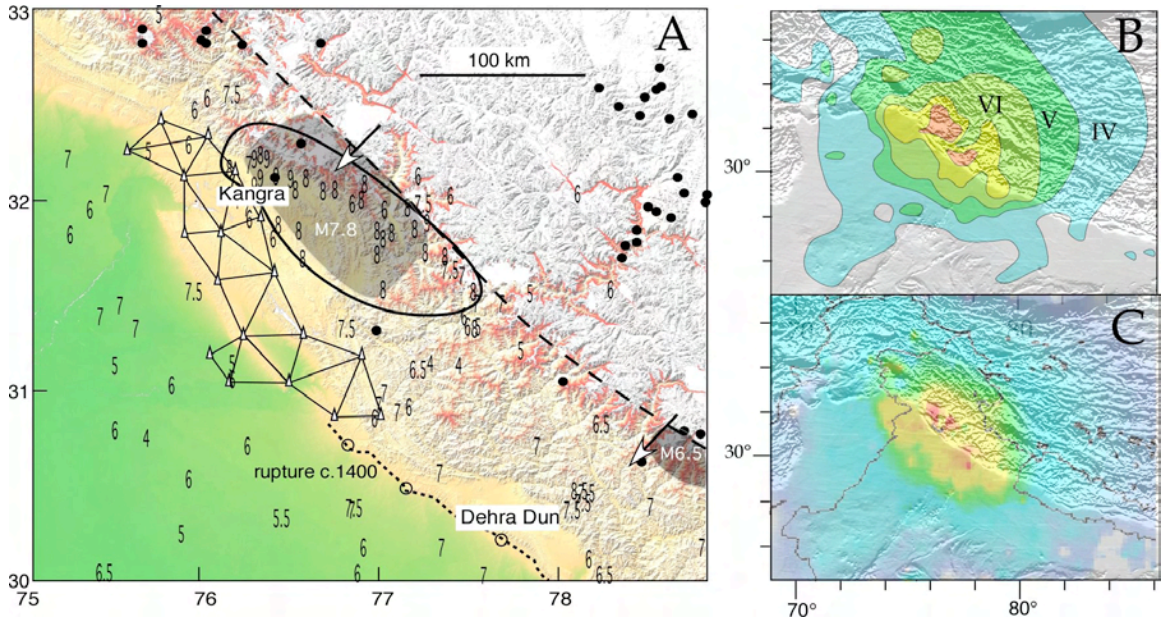

Fig. 2A) The inferred Kangra rupture area (grey rectangle), triangulation lines, and with an envelope surrounding the Intensity VIII MSK intensities (Bilham & Wallace, 2005) Black circles are earthquakes greater than Mw5 and arrows indicate GPS convergence directions. 2B) MSK intensities contoured as conventional isoseismals using kriging methods. 2C) colour-contoured intensity distribution using the methods outlined in the text using same color coding as in 2B. Note the two separate Intensity VIII areas caused by a triggered earthquake near Dehra Dun in the coda of the mainshock (Hough et al., 2004).

4 April 1905 Kangra Mw7.8

A triangulation network samples the SW corner of the inferred 1905 rupture and provides weak constraints for an inferred shallow-dipping thrust fault with 4±1 m of slip (Wallace et al., 2005). We assume that the rupture propagated from NW to SE (Fig 2a). Although the rupture parameters are not well constrained by the geodetic data (Table 1), the quantitative conclusions of all 20th century articles on the Kangra rupture can be rejected because they were invariably based on faulty data. We explain briefly the historical reasons for these erroneous previous conclusions.

Several authors have used leveling data from the Dehra Dun region to support the notion that rupture extended 250 km SE of the epicenter, consistent with a region of high intensity shaking recorded in the region of Dehra Dun, most recently by Yeats et al., (1992). A re-evaluation of the raw leveling data shows, however, that the leveling data have systematic errors (Bilham, 2001) and that there was probably little or no uplift in the Dehra Dun region. The absence of horizontal deformation of triangles near Dehra Dun independently confirms this conclusion, and indicates that rupture fell far short of 180 km. This is consistent with the revised magnitude of Mw=7.8, which suggests the rupture length was no more than 110 km (Wallace et al., 2002) corresponding approximately to the zone of re-evaluated MSK intensity VIII. The rupture presumably terminated to the southwest near the mapped location of the Jawalmucki thrust fault (Powers et al., 1998; Wallace et al, 2005), and to the north near the geodetic locking line that approximately follows the 3.5 km contour (Avouac, 2003).

Previous attempts to assess the location, extent and strike of the 1905 rupture area

based on published intensities (Middlemiss, 1910) show a zone of intense destruction near the town of Kangra (RF VIII-X), and an isolated zone of lower intensity (RF VIII) ~250 km to the SW near Dehra Dun. For many years the early inflated magnitude estimates of Middlemiss et al., (1910) supported the widely-held belief that the rupture zone corresponded to the area of RF intensity VII shaking that enveloped these two regions.

The reality of the intervening region of lower intensity shaking between these two regions of damage was investigated by Seeber and Armbruster, 1981 and Molnar, 1987. who concluded that Middlemiss's coverage of the intervening region would have revealed high intensity shaking had any been present. We revisit this issue using our revised and expanded MSK data. We contour the reevaluated MSK distribution using a mathematical algorithm. Contouring is done using the GMT routine "surface" (Wessel and Smith, 1991); this routine produces contours of randomly spaced spatial data, z(x,y), by solving

$$(1-T)*L(L(z)) + T*L(z) = 0 \qquad \ldots.(1)$$

where T is a tension factor and L is the Laplacian operator. We use T=1, which provides a harmonic solution with no maxima or minima away from control points. Our contours resemble the older Rossi-Forel isoseismals, although our larger number of intensity reports reveals additional detail. The contours in Figure 2B & C confirm the low intensity region separating the epicentral rupture zone from a zone of high intensity near Dehra Dun. The reinterpreted macroseismic data thus provide independent corroboration for the rupture parameters inferred from geodetic data.

A further note regarding the results shown in Figure 2B & C is that Middlemiss' highest Rossi-Forrel isoseismals tend to include unjustifiably large areas, a conclusion derived also for Oldham's raw isoseismals contoured for the 1897 earthquake (Ambraseys and Bilham, 2003). This bias is caused by extensive building damage at relatively modest levels of shaking. A comparison of Middlemiss' areas of Rossi-Forel shaking with those of inferred MSK shaking shows them to be approximately one intensity unit too high above Intensity VIII and a half intensity too high above intensity VII. For lower intensities we find the areas comparable.

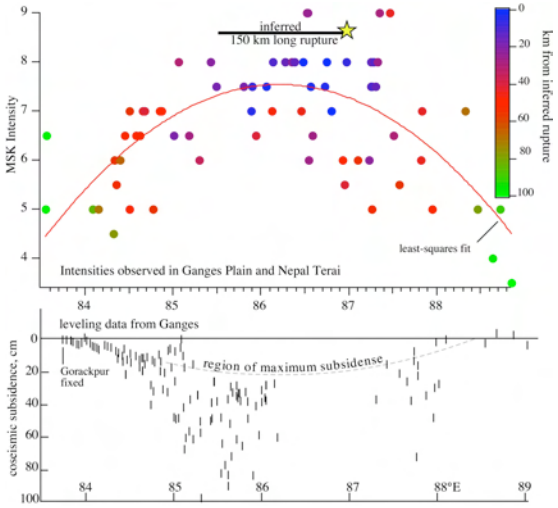

Fig. 3 MSK Intensity and bench-mark subsidence in northern India plotted versus longitude, compared to the epicentre determined by Chen & Molnar, 1977) and 160-km line we infer to represent the most likely location for the rupture zone. A least-squares fit of intensity is centered on this line, as is the region of maximum bench mark subsidence.

15 January 1934 Nepal/Bihar Mw8.2

The 1934 earthquake, although the most recent of the three we consider, is the least well- constrained in terms of its rupture area. For half a century following the shock maximum damage was thought to overlie a rupture beneath the Ganga plain in the Bihar province of India, corresponding to early instrumental locations of the epicenter (Gutenburg and Richter, 1954). The relocated epicenter lies approximately 10 km south of Mt. Everest at 27.55°N, 87.09°E (Chen and

Molnar, 1977) who calculate a seismic moment of 1.1×10^{28} dyne cm and a slip of 5.4 m assuming a 130 x 50 km^2 area rupture corresppooinding to Mw=8.0. Ambraseys and Douglas (2003) calculate Mw8.11 for the event which corresponding to dimensions of 150 x 80 km^2 and a slip of 5m. An appraisal of damage in Nepal (Pandey and Molnar, 1988) shows that severe shaking in eastern Nepal was largely unknown to the Survey of India officers who compiled the memoir on the earthquake (Dunn et al., 1939).

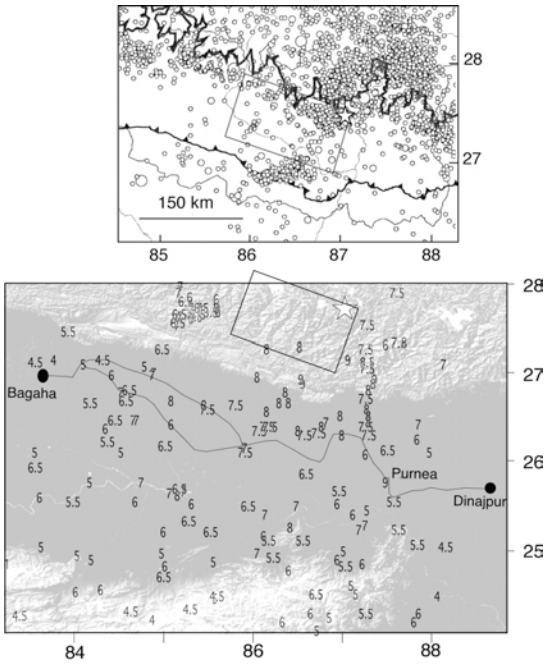

Fig. 4. Seismicity (from Avouac, 2003), MSK intensities & inferred rupture for the 1934 Nepal/ Bihar earthquake. Star indicates Chen and Molnar (1989) epicenter. The microseismicity in southern Neapl between 86 and 87° are mostly aftershocks of the deep Udaypur 1988 earthquake. Our preferred rupture is not well constrained but its SW corner corresponds to a change in strike of the Himalayan front from N110E to N90E at ≈87° E. Bihar leveling lines show subsidence between Bagaha (Goruckpur) and Dinajpur (Figure 3).

No precise geodetic measurements were in place across the 1934 rupture area due to Nepal's political isolation when the Trigonometrical Survey of India was in progress. George Everest's specific requests to use the Nepal foothills for the survey were rejected by the Court of Directors of the East India Company necessitating an elaborate series of masonry towers, many of which were destroyed prior to and during the earthquake. Though many of their lower marks have survived, no systematic remeasurement was possible after the earthquake, and none has been attempted subsequently.

In contrast, first-order spirit leveling lines in northern Bihar were remeasured shortly after the earthquake (Burrard, 1934; DeGraaf Hunter, 1934; Bomford, 1937). Recovered bench-marks measured along the 550-km-long leveling line between 84° and 88° subside by as much as 1.1 m near points that have subsided by less than 0.2 m, and hence the data are considered more a measure of sediment slumping and liquefaction, than a measure of earthquake-related footwall subsidence (Bilham et al. 1998). If this interpretation is correct one might anticipate a correlation between shaking intensity and the degree of subsidence, and this indeed appears to be the case (Figure 3).

Using Chen & Molnar's (1977) relocated epicenter and the region of maximum shaking intensity and subsidence as proxy measures of the centroid of the 1934 earthquake we conclude that the rupture propagated from east to west. This is opposite to the direction calculated by Singh and Gupta (1980). An eastward-propagating rupture appears to us very improbable given the requirements of a 130 to 160-km-long rupture that includes the relocated epicenter, since this would shift the eastern half of the rupture into Sikkim province, where no coseismic deformation has been reported.

Using the above reasoning we constrain the 1934 western edge of the Nepal rupture at 85.5±0.2° and western edge to 87.0±0.2° a distance of ≈160 km with the caveat that its

location may be in error by ±25 km to the east or west (Figure 4). We constrain the northern edge to be the line of microseismicity (Bettinelli et al, 2006; Bollinger et al., 2007) identified with the transition between the shallow-locked and downdip-creeping Indian plate at 15-19 km depth (the locking line of Feldl and Bilham, 2006). We constrain its southern edge to a line 5-10 km north of the frontal thrusts at a depth of 2-4 km since no surface slip was reported. For adopted rupture parameters see Table 1.

Table 1 Rupture parameters adopted for the three earthquakes. The 1897 rupture plane of the inferred Oldham Fault dips steeply at 50±10°SSE. The Chedrang fault slipped to the surface, down to the west with maximum 10 m of slip in the NW tapering to <1 m 35 km to the south. Slip on the 1905 and 1935 are ruptures are assumed to have occurred on 6±2° planes dipping NW or NNW normal to their strike. We asume 90°rake in each case.

Rupture	SW lat.	SW long.	Depth km	NE lat.	NE. long	Depth km	Length km	Width, km	Slip m	Mw
1897Oldham	25.7±0.1	91.6±0.1	35±5	25.6±0.1	91.7±0.1	9±1	110±10	35±10	16±5	8.1
Chedrang F.	25.9	91.7	0	25.7	90.75	9±1	35±5	9	1-10	7.1
1905 Kangra	32.1±0.1	76.2±0.1	5±1	31.9±0.2	77.3±0.2	17±2	100±20	55±10	4±1	7.8
1934 Nepal	26.2±0.1	85.5±0.2	3±1	26.7±.1	87.0±0.2	17±2	150±25	85±10	5±1	8.1

Predicted Intensity Distributions

One can use modern modeling methods to predict the distribution of ground motions from a given fault model and, using established relationships between ground motions and intensities (e.g., Wald et al., 1999) and convert this into a predicted damage map (e.g., Hough et al., 2002). We calculate predicted hard-rock damage patterns from both the 1897 and 1905 earthquakes using rupture models constrained from geodetic data and other available information. Because the rupture geometry of the 1934 event is less well-constrained, we will explore different scenarios for this event. We use a well-calibrated, semi-stochastic approach that includes finite-fault effects to the extent that the source is distributed, although finite-fault phase effects are not modeled with this approach (Beresnev and Atkinson, 1997). We also initially use the attenuation results of Singh et al. (1999) for regional Q(f). Geometrical spreading is included in the model as well: we assume a r^{-1} decay from 0 to 50 km and a $r^{-0.5}$ decay at greater distances. One key unknown in the modeling approach is the "strength factor," S_f, which is related to slip velocity, v_m, according to

$$v_m = 0.618 y (\delta\sigma) S_f / (\rho\beta) \quad \text{--------- (2)}$$

where y is the rupture-propagation velocity, β is the shear-wave velocity, $\delta\sigma$ is the subevent stress drop, and ρ is density (Beresnev and Atkinson, 2001). For all earthquakes we initially choose the same value obtained previously for the Bhuj earthquake: 1.6 (Hough et al., 2002). This value is in the middle of the range estimated by Beresnev and Atkinson (2001) for earthquakes in eastern North America. Although S_f cannot be determined precisely without quantified ground motion estimates, it can be adjusted based on the overall intensity pattern. For the 1897 earthquake, we find that the value of 1.6 provides a very good fit to the extent of the region over which light damage occurred. For the 1905 and 1934 earthquakes, a better fit is obtained with slightly lower values: 1.2 and 1.4, respectively. We note this leads to an intriguing but speculative suggestion that low-

angle ruptures are characterized by a lower strength factor—i.e., a slower slip velocity—than high-angle ruptures such as Bhuj and Assam. The suggested difference is on the order of 30%.

Given the inherent limitations associated with modeling macroseismic (as opposed to modern waveform data), we embark on modeling exercises not to draw quantifiable conclusions about source properties but rather as the best way to establish a hard-rock intensity field against which we can infer residuals. The Beresnev and Atkinson (1997) approach allows us to include our best estimate of path and source parameters to derive shaking levels; the results are thus more physically based than a more empirical approach would be. Our approach does, however, include an empirical component as well: parameters are chosen to yield an overall match to observed intensities in regions where no significant site response is expected.

To include the effect of seismic slip on the Chedrang fault rupture in our predicted shaking map for the 1897 earthquake, we model a second event with its estimated rupture parameters (Table1). Slip on the Chedrang Fault may have occurred within a few minutes of the mainshock as a Mw7.1 sub-event, or it may have occurred as one of the larger aftershocks, or it may have slipped aseismically over many days or weeks, since it was not mapped for many months after the mainshock. The largest aftershock (2 August 1897) was calculated to be Mw6.2 (Ambraseys and Douglas, 2004) with an inferred causal geometry and slip an order of magnitude too small to account for the maximum 10 m slip and >35 km length of the Chedrang Fault had this slipped seismically.

The combined intensity map is then determined by choosing, at each point, the higher of the values predicted from the Chedrang and Oldham fault ruptures. This approach presumably provides a lower bound for the combined shaking level, as two distinct ruptures are expected to prolong the duration of strong ground motion at many sites, and thus to potentially generate more severe damage than two distinct earthquakes.

For the 1934 earthquake we have the additional complication of uncertainty in rupture geometry and location. We therefore explored several different rupture scenarios for this event, starting with a long rupture (200 km) centered on the epicenter proposed by Molnar (1987). Although different choices of strength factor and attenuation can have a substantial effect on the predicted intensities, we conclude that a 200-km rupture does not provide a good fit to the observed MSK data because it overpredicts the swath of highest intensities. In particular, if the rupture extends westward to near the Kathmandu valley, our modeling predicts greater damage than was observed.

We are able to best match the overall intensity distribution with a 150-km rupture length, an 80-km width, and a dip of 6 degrees. The data can be well fit with two different rupture locations: one striking N285E from an endpoint at 26.8N, 87E and one with a strike of N271E from an endpoint of 26.95N, 87.7E.

In addition to the rupture geometry uncertainties, our modeling of the 1934 earthquake revealed persistent trends with distance in the MSK residuals. The Q(f) model of Singh et al. (1999) results in MSK residuals that are increasingly negative to the southeast of the rupture and increasingly positive in other directions, particularly along the Himalayan arc. We conclude that the Singh et al. (1999) Q(f) model is slightly too low for Himalayan paths and too high for paths extending to the southeast outside of the Indian shield. Our final modeling results thus employ two different Q(f) models: $Q=400f^{0.48}$ for locations to the southeast and $Q=750f^{0.48}$ for other locations. As with the 1897 and 1905 events, MSK residuals are calculated relative to predictions from our preferred source and attenuation models (Figure 5.)

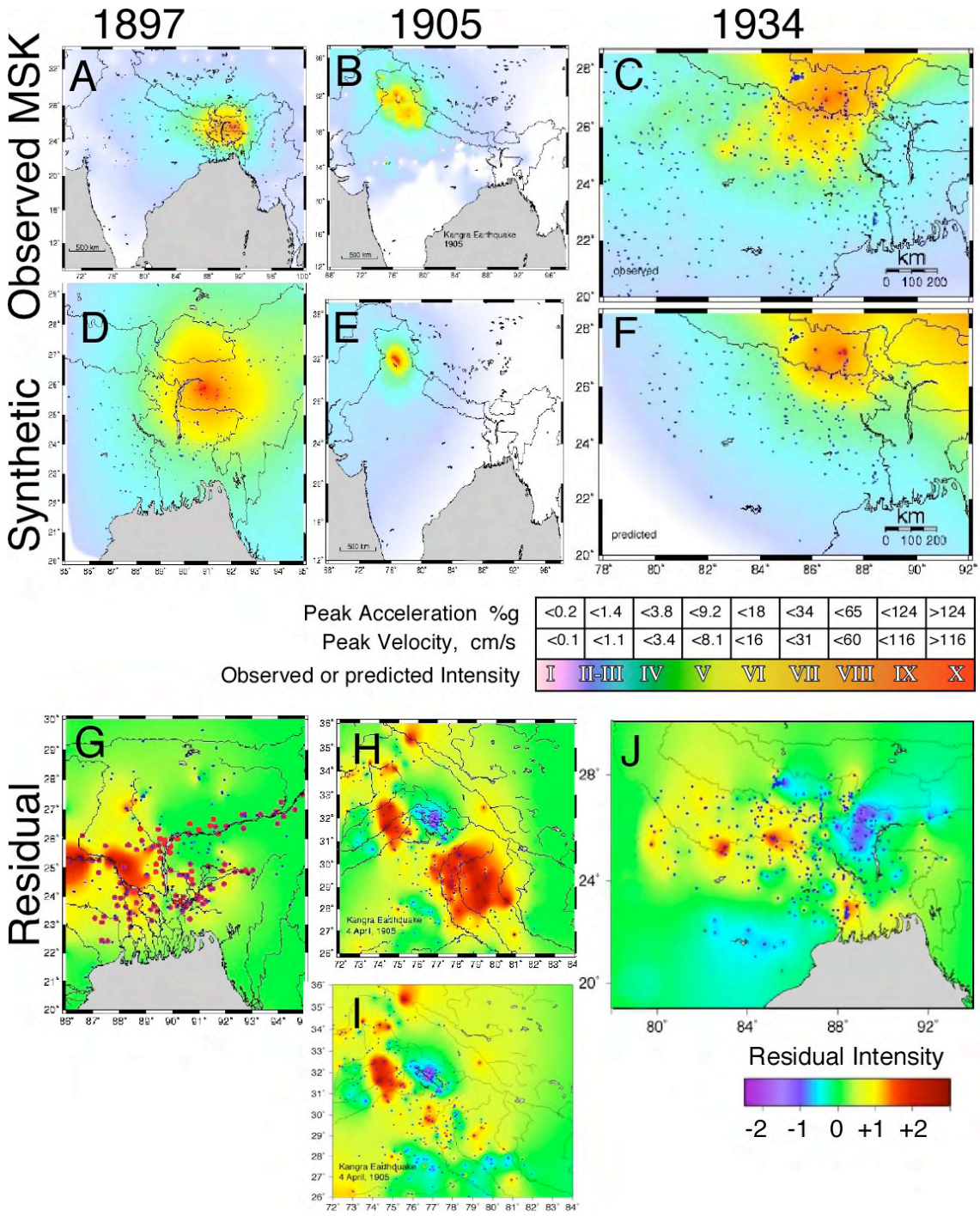

Fig. 5. Observed MSK and synthetic intensity distributions for the 1897, 1905, and 1934 earthquakes and their residuals. Dots in A-F indicate locations of observed intensities. In the 1897 residual map (G), points where liquefaction was observed show up as isolated "spots". A halo is visible around the 1905 epicenter (5H) with a large red area in the SSE corresponding to an inferred triggered M7 earthquake in the lower-crust. We emulate this triggered event and form a new residual (5I). The basin response in 1934 reveals amplification throughout the Ganges basin (5J) with an amplified shoaling effect near its southern edge. A region of subdued intensities overlies the region of shallow surface cover (<100 m in places) west of the Shillong plateau, that may in part be caused by the westward directivity for the 1934 rupture.

Uncertainties in source parameters and propagation effects will invariably limit our ability to resolve site response. In effect, however, our modeling approach provides a basis for "curve fitting" the MSK data in a way that accounts explicitly for such factors as finite-fault effects and attenuation. (The Beresnev and Atkinson (1997) method does not reproduce directivity phase effects, but does reproduce amplitude effects via the subevent summation.) An alternative, strictly empirical approach would be to simply use the MSK data to determine a reference hard-rock attenuation curve directly, and then use this curve to determine residuals and site response. We have explored this type of analysis but conclude that the modeling approach, even with its attendant uncertainties, is preferable because it is more physically based. That is, whereas the empirical approach would require us to assume a parametric form for the decay of intensity with distance, the modeling approach instead employs a Q(f) function.

For the 1897 Shillong earthquake, we obtain a broad region of amplified intensities corresponding to the Ganges Basin (Figure 5A & G), consistent with the expectation of amplification at soft-sediment sites. We do not observe amplification along the Brahmaputra River, but this of course does not signify that it did not occur. Our conclusions here are limited by the rejection of numerous observations for which there was documented liquefaction, but insufficient information to assign intensity (Ambraseys and Bilham, 2003). Many of the liquefaction sites are along the Brahmaputra River (figure 5G); it thus appears that shaking was amplified in these locations as well but the observations are not sufficient to quantify it. Throughout the Ganges Basin, however, we find consistent amplification of 1-2 intensity units, implying a peak ground acceleration amplification of 2-4 (Wald et al., 1999; Hough, 2000).

The intensity residuals from the 1905 earthquake reveal a more complex pattern than those from the 1897 event (Figure 5H & I discussed below). Our preferred choice of strength factor results in a good overall match to the shaking distribution. However, several features of the residual map are found to be insensitive to changes in modeling parameters.

We make the following observations: 1) Shaking in the main rupture zone is overpredicted, 2) amplified shaking is observed near the banks of rivers in the Ganges, and in the Kashmir Valley, 3) a faint region of increased intensity is evident surround the epicenter at a distance of roughly 180 km, and 4) a broad region of high residuals is found near Dehra Dun; this is displaced 20 km to the east from a high intensity zone contoured by Middlemiss. These observations are discussed below.

Our modeling predicts stronger near-field shaking than that observed in the Kangra region. It is possible that this reflects a bias in the intensity assignments: if the only structures damaged in an earthquake are of construction types that are highly vulnerable to damage, it is impossible to ascertain if very high shaking occurred. However, the 1905 mainshock is inferred to have been a low-angle thrust rupture of the main Himalayan decollement fault, and several recent studies suggest that other shallow thrust events, most notably the 1999 Chi-Chi, Taiwan earthquake, generated relatively low near-field peak accelerations (e.g., Boore, 2001). Our results are consistent with this hypothesis.

Our second observation, of amplified shaking along rivers and in valleys, is again consistent with expectations for significant amplifications at soft-sediment sites. The degree of amplification is consistent with that inferred for the 1897 earthquake.

The faint high-intensity "halo" surrounding the mainshock extends both to the west of the

mainshock, on sediment sites, and to the east, on hard-rock sites. Hough et al. (2004) interpret this pattern as evidence that post-critical Moho reflections are large enough to contribute in a significant way to damage patterns. Previous studies have argued for such an effect in other earthquakes beginning with the 1989 Loma Prieta, California earthquake (Somerville and Yoshimura, 1990). Somerville and Yoshimura (1990) showed that SmS arrivals were larger than the direct S arrivals at distances of 50-100 km; later studies (e.g., Mori and Helmberger, 1996) have found similar results. Although a detailed crustal model would be required for precise ray-tracing, tomographic studies indicate that the Moho is located at approximately 40 km along the Himalayan front (Wu et al., 2003); high amplitude SmS waves at distances of 100-200 km are thus consistent with this interpretation.

Perhaps the most conspicuous feature in the residual 1905 intensity plot (figure 5H) is the roughly circular region of high intensities near Dehra Dun, centered slightly to the west of Middelmiss' intensity VIII outlier. Given the instrumental evidence for a sizable triggered earthquake following the 1905 mainshock, we model the intensities from a second mainshock and correct the "mainshock" MSK data by subtracting the predicted intensities caused by a triggered event from figure 5H (figure 5I). To generate the predicted intensities for the triggered event we use M7.1, with an epicenter at 30.4N, 78E, a rupture length of 50 km and a depth to the upper fault edge of 35 km. These parameters are chosen so that the corrections result in small final residuals at hard rock sites in the Dehra Dun region. The circular nature of the residual intensity pattern (figure 5I) is suggestive of a triggered earthquake rather than sedimentary basin amplification since at least half of the high intensity observations are found north of the Ganga Plain within the Himalayan foothills. This is discussed at length by Hough et al. (2004).

The residual for the mainshock and triggered shock show a halo around the mainshock that we have interpreted as a S-wave that has reflected back to the surface from the Moho at an angle lower than critical angle required to pass into the mantle (Hough et al. 2004). While a number of studies have found evidence that post-critical Moho reflections contribute to damage patterns, past studies have relied on far fewer data points than are provided by our dense sampling. For perhaps the first time, dense macroseismic data have illuminated the full spatial distribution of SmS arrivals. These results suggest a deeper Moho to the northeast of the mainshock than to the southwest, a hypothesis that will be testable when crustal structure is known in more detail.

A faint halo is suggested in the intensity residuals calculated for the 1897 earthquake, especially to the south and west of the epicenter. The signal is less prominent, however, than that of the 1905 earthquake, presumably due to the latter event's substantially deeper epicenter and different mechanism. For the 1934 event there are virtually no MSK values at appropriate distances to the north and west of the mainshock, and no halo is observed (figures 5C & 5J).

Our preferred modeling result for the 1934 earthquake yields the residual map shown in Figure 5J. The rupture and propagation parameters have been chosen to yield sensible residuals at (presumed) hard-rock sites at large distances. The most notable features of the residual map are a conspicuous region of low observed intensities to the east/ southeast of the mainshock and, once again, amplification of 1-2 units within the Ganges basin, with especially strong amplifications immediately adjacent to rivers. The former result is suggestive of a directivity effect, with rupture directivity towards the west. This is contrary to the results of Singh and Gupta (1985); however their conclusions are based on limited waveform data.

Finally, we combine the MSK residuals from all three earthquakes to obtain a site response map for the Ganges basin and its environs (Figure 6). Such a compilation will reflect some propagation effects that might be unique to individual earthquakes, for example a SmS "halo" from the 1905 mainshock and directivity effects from the 1934 earthquake. Although the combined site response map will still reflect some source/path effects, we conclude that the residuals primarily reflect site response; a compilation thus allows us to put together, essentially, a preliminary site response map for much of northern India (Figure 6). This map could be augmented with residuals from other, smaller earthquakes for which reliable macroseismic interpretations are available.

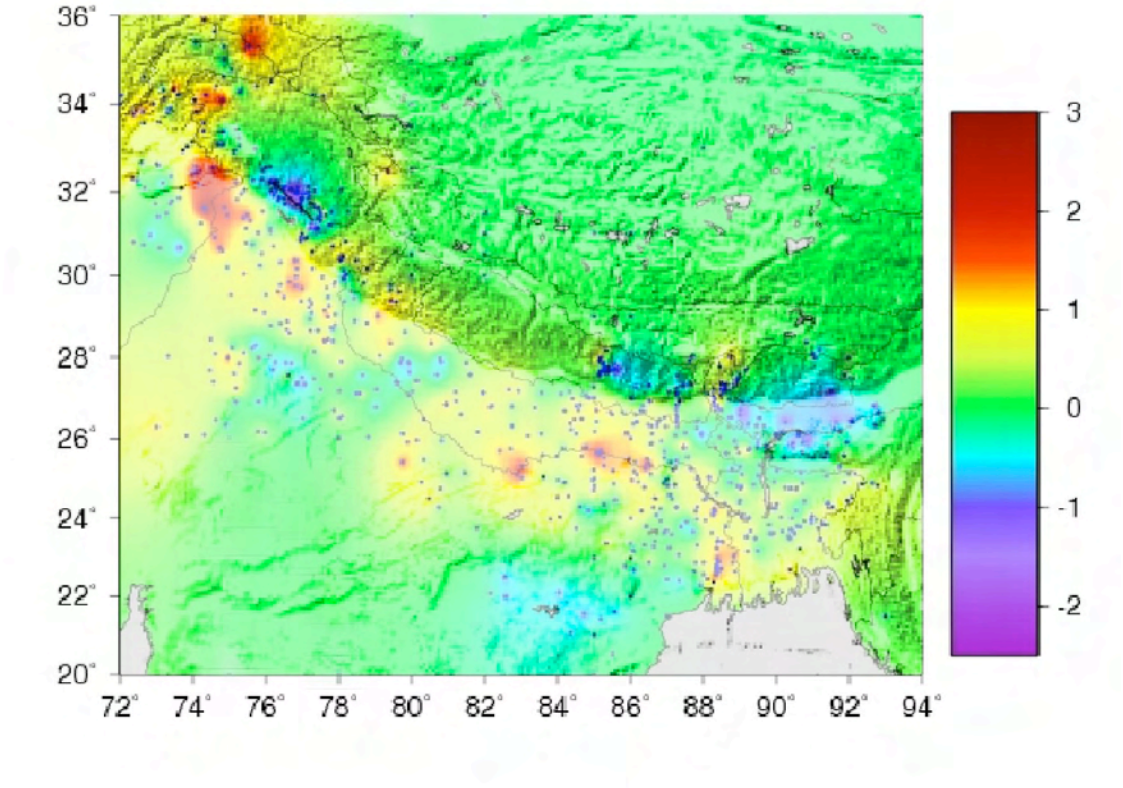

Fig. 6. Residuals for all three events superimposed on shaded relief topography. Points indicate locations of observations. Scale indicates ±3 intensity units.

Discussion and Conclusions

Macroseismic observations from three major earthquakes in the Himalayan region reveal unexpected details of the nature of the ground motions generated by these events. Using available rupture models, we are able to predict the distributions of shaking from the events and to compare these results to the observed intensities. We obtain several interesting results, including maps of sediment-induced amplification in the Ganges Basin and elsewhere, as well as compelling evidence that the 1905 Kangra mainshock was followed by a subsequent, remotely triggered earthquake in the Dehra Dun region. The depth of this triggered earthquake (30-50 km) requires it to have occurred below or near the base of the Indian plate.

We infer the location of the rupture zone of the 1934 Mw8.1 earthquake from the distribution of maximum intensities observed in Nepal and Bihar, and infer also a westward propagating rupture from the disposition of the intrumental epicenter relative to these intensities. Our preferred location places the front edge of the rupture parallel to the strike of the range west of the Arun River. The location of the rupture zone of this important earthquake has been uncertain in the past due to the absence of geodetic data or aftershock locations. Although independent verification of the edges of this rupture (with approximate estimated dimensions of 150 x 85 km^2) is unavailable, the resemblance between our forward model of shaking intensities and the observed shaking, provides a measure of confirmation of the essential correctness of the location and strike of the rupture.

From the data available from the three earthquakes we have considered we conclude that shaking intensities above the ruptures of Himalayan earthquakes are invariably equal or in excess of intensity VIII, and that these high intensities extend far into the adjoining sedimentary basins. A trivial conclusion is that archaeological sites in the Himalaya and in the northern Ganges and Punjab plains will have experienced this level of shaking, possibly several times in the past 1000 years, assuming a recurrence interval of approximately 500 years (Feldl and Bilham, 2006). We further note that no great earthquake has ruptured the frontal thrusts of the Himalaya in the past two centuries (although the 2005 Mw 7.6 Kashmir earthquake was associated with a surface rupture), and yet very large historical surface ruptures (>20 m of surface slip) have been recorded both in Nepal and in the western Himalaya, and that these must be associated with much larger earthquakes than those analyzed here.

The extrapolation of weak-motion site response results to the strong motion regime is always plagued by uncertainties regarding the degree of non-linearity associated with strong-motion sediment-induced amplification. Although ground motions (peak amplitudes and/or durations) are expected to be larger for rare great events exceeding Mw8.5, the amplifications estimated from large (Mw7.8 to 8.1) are presumably more reliably extrapolated than amplifications estimated from instrumentally recorded small and moderate events.

Acknowledgements

We gratefully acknowledge the important contribution of Nick Ambraseys who has unified the analysis of intensities for the three historical earthquakes which we have investigated. Support for RB came from National Science Foundation Grants EAR0229690 and NSF EAR0003449. Any opinions, findings, and conclusions or recommendations expressed in this paper are those of the author(s) and do not necessarily reflect the views of the National Science Foundation.

Bibliography

Ambraseys, N., 2000. Reappraisal of north-Indian earthquakes at the turn of the 20th Century, Curr. Sci., 79: 1237-1250.

Ambraseys, N. and R. Bilham, 2000. A note on the Kangra Ms=7.8 earthquake of 4 April 1905. Curr. Sci, 79: 101-106.

Ambraseys, N. and R. Bilham, 2003. MSK Isoseismal intensities evaluated for the 1897 Great Assam Earthquake, Bull. Seismol. Soc. Am., 93: 655-673.

Ambraseys, N. N. and J. Douglas, 2004. Magnitude calibration of north Indian Earthquakes, Geophys. J. Int., 159: 165-206.

Avouac, J.P., Mountain Building, Erosion, and the Seismic Cycle in the Nepal Himalaya, *Advances in Geophysics*, Vol. 46, 10.1016/S0065-2687(03) 46001-9, December 2003.

Bettinelli, P., J-P Avouac, M. Flouzat, F. Jouanne, L. Bollinger, P. Willis, G. R. Chitrakar, 2006. Plate motion of India and interseismic strain in the Nepal Himalayafrom GPS and DORIS

measurements. *J. Geod*. doi:10.1007/s00190-006-0030-3

Bollinger, L., F. Perrier, J.P. Avouac, S. Sapkota, U. Gautam, and D.R. Tiwari, 2007. Seasonal modulation of seismicity in the Himalaya of Nepal *Geophys. Res. Lett.,* 34, L08304, doi: 10.1029/2006GL029192.

Boore, D.M., 2001. Comparisons of ground motions from the 1999 Chi-Chi earthquake with empirical predictions largely based on data from California, Bull. Seismol. Soc. Am., 91, 1212-1217.

Burrard, S., 1934. Ground levels in Bihar in relation to the earthquake of January 15 1934.*Nature(Lond),* 582-583.

Beresnev, I.A. and G.M. Atkinson, 1997. Generic finite-fault model for ground-motion prediction in eastern North America, *Bull. Seismol.. Soc. Am*., 89: 608-625.

Bilham. R., F. Blume, R. Bendick and V. K. Gaur. Geodetic constraints on the Translation and Deformation of India: implications for future great Himalayan earthquakes, 1998, *Current Science*, 74,(3), 213-229.

Bilham, R., 2001. Slow tilt reversal of the Lesser Himalaya between 1862 and 1992 at 78E and bounds to the southeast rupture of the 1905 Kangra earthquake, Geophys. J. Int, 144: 1-23.

Bilham, R. and P. England, 2001. Plateau pop-up during the great 1897 Assam earthquake, Nature, 410: 806-809.

Bomford, G., 1937. Leveling in Bengal and Bihar, 93-97. *in* Couchman, H. J., Survey of India Geodetic Report, 1936, Geodetic Branch Survey of India, Dehra Dun, 1937. pp. 97.

Boore, D.M., 2001. Comparisons of ground motions from the 1999 Chi-Chi earthquake with empirical predictions largely based on data from California, Bull. Seismol. Soc. Am., 91: 1212-1217.

Chen, W-P and P. Molnar, Seismic moments of major earthquakes and the average rate of slip in Central Asia, Geophys. Res., 82, 2945-2969, 1977.

Chen, W.-P. and H. Kao., Seismotectonics of Asia: Some recent progress, in the *Tectonic Evolution of Asia*, ed. A. Yin and T.M. Harrison, Cambridge University Press, 1996, 37-54.

De Graff-Hunter, J. , 1934 The Indian earthquake (1934), *Nature(Lond)*, 236-237.

Dunn, J. A., J. B. Auden, A. M. H. Ghosh, S. C. Roy & D. N. Wadia (1939). The Bihar-Nepal Earthquake of 1934, Mem/ Geol Surv. India, 73, 1-391.

Feldl, N and R. Bilham, Great Himalayan Earthquakes and the Tibetan Plateau, *Nature* 444, 165-170 (9 November 2006) | doi:10.1038/nature05199.

Gutenberg, B., and C.F. Richter, 1954. Seismicity of the Earth and Associated Phenomena, Princeton University Press, Princeton, 310pp.

Hough, S.E., On the scientific value of "unscientific" data, Seismol. Res. Lett., 71, 483-485.

Hough, S.E., S. Martin, R. Bilham, and G. Atkinson, 2002. The 26 January, 2001 Bhuj, India earthquake: observed and predicted ground motions, Bull. Seismol. Soc. Am., 92: 2061-2079.

Hough, S.E., R. Bilham, N. Ambraseys, and N. Feldl, 2004. Revisiting the 1897 Assam and 1905 Kangra earthquakes in northern India: Site response, Moho reflections, and a triggered earthquake, Current Science 88, 1632-1638.

Middlemiss, C.S., Preliminary account of the Kangra earthquake of 4 April 1905, 1905. Mem. Geol. Soc. India, 32, Pt. 4: 258-294, Geol. Surv. India, Calcutta.

Middlemiss, C.S., The Kangra earthquake of 4 April 2005, 1910. Mem. Geol. Surv. India, 38: 405.

Molnar, P., The distribution of intensity associated with the 1905 Kangra earthquake and bounds on the extent of rupture, 1987. J. Geol. Soc. India: 29, 221.

Mori, J. and D. Helmberger, Large-amplitude Moho reflections (SmS) from Landers aftershocks, southern California, 1996. Bull. Seismol. Soc. Am., 86: 1845-1852.

Nandy, D.R., A.K. Cloudhury, C. Chakraborty, and P.L. Narula (1993). Geologic Survey of India,

Bihar-Nepal earthquake, August 20, 1988, Sp. Pub. Geol. Surv. India 31.

Oldham, R.D., 1899. Report on the great earthquake of 12th June 1897 (incl. the reports by P. Bose, G. Grimes, H. Hayden, T. LaTouche, and E. Vredenburg), Mem. Geol. Surv. India, 29, pp. 1379, Calcutta.

Pandey, M. R., and P. Molnar, The distribution of intensity of the Bihar-Nepal earthquake of 15 January 1934 and bounds on the extent of the rupture zone, *J. Geol. Soc. Nepal,* 5, 22-44, 1988.

Powers, P. M., Lillie, R. J., and Yeats, R.S. 1998. Structure and shortening of the Kangra and Dehra Dun reentrants, sub-Himalaya, India, Geol. Soc. Am. Bull., 110: 1010-1027.

Seeber, L. and J.G. Armbruster, 1981. Great detachment earthquakes along the Himalayan arc and long-term forecasting, in Earthquake Predictionan International Review, eds. D.W. Simpson and P.G. Richards, Maurice Ewing Series, Am. Geophys. U., 4: 259-277.

Singh, D. D. and H. K. Gupta, (1980)
Source dynamics of two great earthquakes of the Indian subcontinent; the Bihar-Nepal earthquake of January 15, 1934 and the Quetta earthquake of May 30, 1935. *Bull. Seism. Soc. Am*, 70(3): 757-773

Singh, S.K., M. Ordaz, R.S. Dattatrayam, and H.K. Gupta, A spectral analysis of the 21 May 1997, Jabalpur, India, earthquake (Mw=5.8) and estimation of ground motion from future earthquakes in the Indian shield region, 1999. Bull Seismol. Soc. Am., 189: 1620-1630.

Somerville, P. and J. Yoshimura, The influence of critical Moho reflections on strong ground motions recorded in San Francisco and Oakland during the 1989 Loma Prieta earthquake, 1990. Geophys. Res. Lett., 17, 1203-1206.

Wald, D.J., V. Quitoriano, T.H. Heaton, and H. Kanamori, 1999. Relationships between peak ground acceleration, peak ground velocity, and modified Mercalli intensity in California, Earthquake Spectra, 15: 557-564.

Wallace, K.; Bilham, R.; Blume, F.; Gaur, V. K.; Gahalaut, V.,(2005) Surface deformation in the region of the 1905 Kangra Mw = 7.8 earthquake in the period 1846–2001, *Geophys. Res. Lett.*, **32** (15), L15307, 10.1029/2005GL022906

Wessel, P. and W.H.F Smith, 1991. Free software helps map and display data, EOS, Trans. Am. Geophys. U., 72: 441, 445.

Wu, F., A. Sheehan, G.C. Huang, and G. Monsalve, 2003. Source mechanisms, seismicity, and velocity structures in the Himalayan region, Indo-US Workshop on Seismicity and Geodynamics, 49, Hyderabad.

Yeats, R.S., T. Nakata, A. Faraj, M. Fort, M.A. Mirza, M.R. Pandey, and R.S. Stein, 1992. The Himalayan frontal fault system, Ann. Tect., 6: 85-98.

Journal Earth Systems Science
in press Oct 2007.

Susan E. Hough,
U.S. Geological Survey,
525 South Wilson Avenue,
Pasadena, California, 91106 USA

Roger Bilham:
Cooperative Institute for Research in Environmental Sciences and
Department of Geological Sciences,
University of Colorado at Boulder,
Boulder, Colorado 80309-0399 USA